Nano-objects synthesized from Cu, Ag and Cu28Ag72 electrodes by submerged discharges in liquid nitrogen

H. Kabbara, J. Ghanbaja, C. Noël, T. Belmonte

NANO-OBJECTS SYNTHESIZED FROM Cu, Ag and $Cu_{28}Ag_{72}$ ELECTRODES BY SUBMERGED DISCHARGES IN LIQUID NITROGEN

H. Kabbara[1], J. Ghanbaja[1], C. Noël[1,2], T. Belmonte[1,2,*]

[1]Université de Lorraine, Institut Jean Lamour, UMR CNRS 7198, NANCY, F-54042, France

[2]CNRS, Institut Jean Lamour, UMR CNRS 7198, NANCY, F-54042, France

* corresponding author. Email: thierry.belmonte@univ-lorraine.fr

PACS number: 52.80.Wq Discharge in liquids and solids

Keywords: Spark discharges ; submerged discharges ; 2D materials ; Alloy nanostructures

ABSTRACT

Discharges in liquid nitrogen between 2 electrodes made of either Cu, Ag or $Cu_{28}Ag_{72}$ enable the production of several types of comparable nano-objects. First, Cu nanoparticles (NPs) with sizes close to 5±4 nm nm and 40±10 nm are obtained with Cu electrodes and get oxidized in the air to form CuO after liquid evaporation. With $Cu_{28}Ag_{72}$ electrodes, copper contains a small amount of silver that inhibits oxidation. Next, silver nanoparticles are spherical but when doped with copper, they are facetted. Silver-containing nanowires have very similar features whether they are synthesized with silver or CuAg electrodes. They are made by assembly of NPs. Ag nanosheets are either single crystals in the case of CuAg electrodes or assembly of NPs in the case of silver electrodes. Finally, silver nanorods with traces of copper are only found with CuAg electrodes.

Time-resolved optical emission spectroscopy indicates that the optical thickness decreases when copper is added to silver, lines appearing immediately after breakdown and not only after emission of a broad continuum. Emission of lines belonging to the N II system is then observed. The energy deposited being nearly constant, the structure of the discharge is assumed to be changed.

1. INTRODUCTION

Benefiting from the properties of silver without supporting the cost of this element is an issue that can be solved by replacing silver atoms that are not solicited by atoms of another cheaper element. Copper (Cu) is about 100 times cheaper than Ag while possessing comparable bulk properties – its electrical conductivity is only 6% less than that of Ag –. Then, Cu particles have been considered as an ideal substitute for Ag particles.

Using silver to confer bactericidal properties, for instance, to a nanoparticle surface is usually tackled by resorting to core−shell structures. Many studies focused on the synthesis of Cu@Ag structures [1–5]. From a practical point of view, the outer shell, when made of noble metal, passivates the inner metallic core and avoids side reactions like oxidation [6].

The synthesis of alloy nanoparticles has been less studied [7–12]. The Cu–Ag binary phase diagram does not exhibit any intermediate alloy phase between the two solid solutions $Cu_{1-x}Ag_x$ (x < 8.0 wt.%) and $Ag_{1-x}Cu_x$ (x < 8.8 wt.%) – the value of x depending on the temperature at which the alloy was formed –. For this reason, nanoparticles tend to form bimetallic phases instead of alloys, even though it is possible to get the solid solutions just mentioned. Chowdhury *et al.* [8] produced bimetallic Ag:Cu nanoparticles (~5 nm) by DC magnetron sputtering. With increase in annealing temperature, they observed that Cu atoms surface-segregate, thereby increasing the concentration of Ag in the nanoparticle core as a result. Kim *et al.* [12] synthesized bimetallic nanoparticles (~10 nm) by thermal decomposition of $AgNO_3$ and $Cu(C_5H_7O_2)_2$ dissolved in a mixture of oleylamine ($C_{18}H_{37}N$), surfactant, and reducing agent.

These authors proposed a model to explain why Ag:Cu (1:1) particles are less prone to oxidation than copper particles. They found out that a lower adsorption of O_2 molecules is needed in the former case. Valodkar *et al*. [11] used starch to functionalize the metallic nanoparticles with hydroxyl groups, the poor stability of copper as well as alloys being due to the tendency of copper to get oxidized in aqueous medium. Thus, they could stabilize

particles in the aqueous solution, limiting not only their agglomeration but also their oxidation.

Finally, there is no work, to the best of our knowledge, reporting the synthesis of 2D structures made of silver and copper, even though silver is known to have a propensity to grow in two dimensions [13, 14].

In this work, we present results about the synthesis of nano-objects formed by erosion of $Cu_{28}Ag_{72}$ electrodes with spark discharges in liquid nitrogen. This process, whose yields may reach grams per hour, is one of the most efficient to produce nano-objects [15, 16]. The $Cu_{28}Ag_{72}$ is a two-phase mixture: XRD results of the untreated material indicate that it is made of $Ag_{96.4}Cu_{3.6}$ and $Cu_{99.4}Ag_{0.6}$ phases (composition expressed in at.%). These data are compliant with the Ag–Cu binary phase diagram [17] as both compositions correspond to a single temperature (close 510°C). Using spark discharges in liquid nitrogen is a way to produce nanoparticles at high speed, up to several grams per hour. After a short description of the experimental set-up used in this work, we will compare the erosion of silver and copper taken as pure elements and that of the $Cu_{28}Ag_{72}$ alloy. Time-resolved optical emission spectroscopy will be used to investigate the production of metallic vapors during the discharge process.

2. EXPERIMENTAL SET-UP

The experimental set-up was presented in detail in reference [18]. Briefly, a pin-to-pin electrode configuration, immersed in liquid nitrogen, was used. Electrodes were Cu (purity: 99.95%), Ag (purity: 99.99%) or $Cu_{28}Ag_{72}$ (purity: 99.95%) wires (1 mm in diameter). A high DC voltage power supply (Technix SR15-R-1200–15 kV–80 mA) fed a solid-state switch (HTS-301-03-GSM) connected to one pin-electrode, the other electrode being grounded. The voltage rise time was 20 ns without any ballast resistor. The applied voltage of +10 kV and an inter-electrode gap distance of 100 μm were chosen for all experiments.

Nanoparticles are collected by sedimentation on a silicon wafer located under the pin-electrodes. We resorted to scanning electron microscopy (SEM)— XL30S-FEG by Philips— for structural and chemical observations. The XL30S-FEG microscope was equipped with an EDXS (Energy-Dispersive X-ray Spectrometer) used for elemental analysis and a TLD detector (through the lens detector) used for high resolution imaging. A Philips CM200 device and a JEOL ARM 200F Cold FEG device were used for TEM investigation in order to study the crystallinity and the chemical composition of NPs. Copper grids were used for pure silver electrodes but nickel grids were preferred for alloy electrodes in order to avoid any confusion between the copper detected from the synthesized NPs and that detected from the grid..

Optical emission spectroscopy was performed with a 550 mm focal length monochromator (Jobin–Yvon TRIAX 550) equipped with a 100 g mm^{-1} grating for overall spectra in the (250–900 nm) visible range. It was coupled with a HORIBA Jobin–Yvon i-Spectrum Two iCCD detector. Each measurement is averaged over 50 spectra recorded with an exposure time of 50 ns. Although discharges in dielectric liquids are known to be stochastic, the use of the solid-state switch ensures a high level of reproducibility because breakdown necessarily occurs within a time window inferior to the exposure time (see reference [19] for further details). However, because of the generation of high-frequency signals by discharge current oscillations (at about 1 MHz), ghost lines are sometimes observed. They are easily identified in time-resolved data, for they disappear from one spectrum to the other.

3. RESULTS AND DISCUSSION

3.1. Erosion of Cu and Ag electrode

Eroding copper electrodes under the chosen conditions leads to the synthesis of NPs with spherical shapes (**Fig. 1a**). NPs are made of CuO, since copper NPs are exposed to air before analysis, once liquid nitrogen has fully evaporated. According to unreported TEM measurements, these primary NPs have sizes ranging typically between 2 and 10 nm. However, larger primary NPs, with diameters closer to 30–50 nm are also present, but to a

lesser extent. Both types of nanoparticles are produced by condensation of the metallic vapour emitted during the erosion of the copper electrodes (see reference [20] for more details).

Eroding silver electrodes produces 2-dimensional Ag nanostructures together with NPs (**Fig. 1b**). Air exposure does not lead to appreciable oxidation of silver as measured by EDS-X micro-analysis (see **Supplemental material 1**). As for copper, NPs are distributed according to 2 populations in size (**Fig. 2**). Primary NPs have sizes ranging typically between 2 and 8 nm typically (**Fig. 2a**). Larger primary NPs, with diameters closer to 10–30 nm are also present (**Fig. 2b**). Some nanowires, made by self-assembly of nanoparticles of about 20±10 nm in diameter, are observed (circle in **Fig. 3a**). 2-dimensional nanostructures are sheets (**Fig. 1b and Fig. 3a**) that are constituted by self-assembly of nanoparticles of about 20±10 nm in diameter (**Figs. 3a and 3b**).

Experiments were also carried out with one silver electrode and one copper electrode. By creating discharges between two electrodes of different metals, we obtained a mixture of copper and silver objects that were similar to those depicted in **Fig. 1**. Vapours emitted by each electrode do not seem to interact to affect significantly the growth of copper and silver nano-objects. For instance, no alloy could be observed in this case, each kind of objects being made of pure copper or pure silver, within the resolution of EDX measurements.

3.2. Erosion of $Cu_{28}Ag_{72}$ electrodes

Nano-objects produced by erosion of $Cu_{28}Ag_{72}$ electrodes in liquid nitrogen are depicted in **Fig. 4**. Two-dimensional nanostructures (**Figs. 4a** and **4c**), among which few nanorods (~500 nm in length and ~30 nm in diameter) are observed, are found together with crystalline NPs (**Figs. 4b** and **4d**).

Theses NPs are either spherical and then they are rich in copper or silver or they are facetted and only rich in silver. They belong to two different size distributions: one in the range 2–8 nm and one in the range 10–30 nm, like in the case of silver. They are either made of copper with small amounts of silver (**Fig. 5a**) or of silver with small amounts of copper (**Fig. 5b**).

The oxygen content of each type of particles is lower than 5 at.% in average and it is higher on the topmost surface of the particles. The metallic character of both types of nanoparticles was also verified by Electron Energy Loss Spectroscopy (See **Supplemental Material 2**).

Similarly to silver electrodes, erosion of $Cu_{28}Ag_{72}$ electrodes produces 2-dimensional nanostructures, but contrary to the former case, these objects are not an assembly of nanoparticles (**Fig. 6a**). They are dense, without visible sub-structure. Diffraction patterns exhibit monocrystalline structures (**Fig. 6b**) that can be interpreted as the cubic $Ag_{98.5}Cu_{1.5}$ phase after ref. 9016252 of the Crystallography Open Database [21]. This interpretation is in line with the chemical composition of these objects as determined from X-mapping (see also **Supplemental Material 3**, which gives a composition equal to $Ag_{85.5}Cu_{5.5}O_{9.0}$). In **Fig. 7**, the analysis of sheets indicates that they are mainly made of silver but contain traces of copper. A small amount of oxygen is also detected. The large sub-micrometric particle observed in this image has the composition: $Ag_{72\pm2}Cu_{23\pm3}O_{4\pm1}$. Such a large spherical particle is one of these rare particles produced by ejection of liquid from the molten pool that forms during the interaction of the discharge with the electrode. That is why it composition is close to the alloy composition.

In **Fig. 8**, we observe that one-dimensional structures produced from silver (See also **Fig. 3a**) electrodes are also produced from $Cu_{28}Ag_{72}$ electrodes. They belong to the Truss type: in a particle distribution with two sizes, the larger particles serve as connectors between wires of smaller particles, which enables the formation of more complex architectures. X-mapping of these Truss structures indicates that these objects are made of silver and traces of copper and oxygen (See **Supplemental Material 4**).

Finally, a large-view TEM image of nanorods (**Fig. 9a**) as those depicted in **Fig. 4a** shows that these objects are most often attached to sheets. We notice that these nanorods grow from the same root, most often attached to a sheet, with projected angles close to 73° (**Fig. 9b**). They are single crystals (**Fig. 9d**). From the analysis of several nanorods of the kind of that

depicted in **Fig. 9c**, we could show that the orientation of the rods is along the <110> direction. This is within the plane of the sheets that are perpendicular to <002>.

3.3. Optical emission spectroscopy

Comparing discharge emission in liquid nitrogen with silver or with AgCu electrodes gives an interesting picture of the role of copper (**Fig. 10**). At 150 ns, a large and intense continuum is obtained with both types of electrodes (see also **Supplement Material 5**). However, with AgCu electrodes, we observe the overlapping of lines from the N II system, this contribution fading away after a while to be no longer present at 400 ns. It is something we observed already in a former case, with Cu and Zn electrodes (see for details reference [20]). The fact that, at the very beginning of the discharge, no lines from the N_2 I and N I systems are observed is assumed to be due to the optical thickness of the medium. N_2 and N being likely much more concentrated than N^+, only the lines emitted by the excited states of the ion are not trapped – we recall here that for a given optical thickness, the probability of a line to be absorbed is also linked to the concentration of the absorbing states –. After 400 ns, *i.e.* near the transition between the discharge and the post-discharge, silver transitions dominate and are significantly less intense when CuAg electrodes are used. On the other hand, copper lines are difficult to identify because their intensities are very weak. So, copper seems to reduce the optical thickness of the medium at the very beginning of the discharge, which likely might affect the structure of the discharge itself, and the intensity of silver lines. It behaves as an inhibitor of silver production, which is at least partly justified by the dilution effect it induces due its presence at 28% in the alloy.

3.4. Growth mechanisms

If we compare nano-objects grown from silver electrodes to those grown from $Cu_{28}Ag_{72}$ electrodes, we find that (see **Table 1**):

- Cu NPs with traces of Ag are spherical. Ag NPs with traces of Cu are either spherical of facetted. Both are with sizes in ranges: 2–8 nm and 10–30 nm

- Ag with traces of copper nanorods, are only found with CuAg electrodes. They are single crystals of 100s of nm in length.
- Nanowires of Ag have very similar features whether they are synthesized with silver electrodes or CuAg electrodes. They can be several µm in length. They are made of assembly of NPs of 20±10 nm typically.
- Ag nanosheets are 100s of nm in width. They are either single crystals in the case of CuAg electrodes or assembly of NPs of 20±10 nm in the case of silver electrodes.

Basically, the same kinds of objects are produced, except nanorods that are specific to alloy electrodes. Silver objects are better crystallized when copper is present. Instead of an assembly of silver nanoparticles, nanosheets become single crystalline in the presence of copper. Their growth is also associated with the presence of nanorods that are also single crystals.

We cannot rule out the fact that these feature changes from one type of discharge to the other are linked to the structure of discharges, which we know now that it is affected by the use of alloy electrodes. When comparing the electrical signals that characterize the discharge when either 2 silver electrodes or 2 alloy electrodes are used, *i.e.* the time evolution of voltage and current (**Supplemental material 6**), we notice that they are almost identical. Thus, we infer that the plasma volume, its shape and gradients distribution, are modified. However, by lack of information on these changes, we cannot provide at this stage any reliable description of the mechanisms at stake during the growth of silver-rich nano-objects within the discharge.

Furthermore, other effects may contribute to explain the specificity of nano-objects synthesized in the presence of copper.

In the Cu-Ag phase diagram, the addition of 3.6 at.% copper to silver lowers the solidification temperature by about 30 K with respect to pure silver [22]. If we go up to nearly 6 at.% as measured in most of the synthesized objects, the solidification temperature decreases by 60 K, which is not negligible. On the other hand, adding 0.6 at.% of silver to copper does not

decrease significantly the solidification temperature of the alloy. This might explain, at least partly, why copper nano-objects are unaffected by the use of alloy electrode and why silver nano-objects are better crystalline. The temperature needed to solidify nanoparticles being lower, better crystallized objects are produced for a given temperature field. Similarly, it is well known that to sinter NPs, the temperature must be high enough to activate volume diffusion of elements. At lower temperature, surface processes are activated and sufficient to bind particles together. So, with copper in silver, the lowering of the melting temperature might trigger volume diffusion, which would be very limited in pure silver.

Another possible contribution to the best crystallization observed with alloy electrode is the development of stress by copper addition, which would ease the crystallization process. The stress would develop radially, from the center of the nanosheet outwards. In **Fig. 6a**, the photoelastic response of the sheets, which produces the colored interference fringes, is likely due to the presence of stress in these nanostructures. In rarer cases, stress even enables stabilization of allotropic phases in a single object, as shown in the diffraction pattern in **Fig. 11**.

The growth of 2D objects occurs in the gas phase and not on the silicon substrate used to collect the nano-objects. By using a TEM carbon holey grid as substrate, identical results were obtained. This is also deduced from the presence of kinks (easily visible in Fig. 6a) where atoms adsorb to form the object step by step. This feature is also observed with facetted nanoparticles (**Fig. 5b**), which are likely embryos of 2D nanosheets.

The presence of nanorods, *i.e.* crystalline 1D objects, is likely related to the decrease in the solidification temperature. This can be responsible for the inhibition of specific growth directions. As nanorods (see **Fig. 9**) are attached to nanosheets, we may assume that these 1D objects are the result of the time evolution of the nanosheet growth when they move from a hotter to a cooler region. As their growth direction belongs to one of those included in the plane of the sheets, it seems highly probable.

Otherwise, without any seed from a 2D nanosheet, those 1D Truss structures observed in **Fig. 8** are produced. They are made from an assembly of metallic particles available in the discharge. Because, there are several possible ways to assemble nanoparticles into wires, the origin of the anisotropy of these structures must be clarified.

4. CONCLUSION

By comparing discharges in liquid nitrogen ignited between 2 electrodes made of either Cu, Ag or $Cu_{28}Ag_{72}$, we showed that several types of comparable nano-objects could be synthesized. The presence of a few percent of copper in silver leads to better crystallized silver-rich nano-objects, which may be associated with a decrease in the solidification temperature of $Cu_{28}Ag_{72}$ alloy in comparison with silver. This enables the production of facetted silver nanoparticles and the synthesis of 1D single crystal nanorods, which cannot be formed with pure silver electrodes. On the other hand, copper nanoparticles, whether they contain some silver or not, exhibit the same features.

Time-resolved optical emission spectroscopy turned out to be a very useful diagnostics that give access to the structure of the discharge. The appearance of N II lines when copper is present unveils the inner composition of the medium that is not accessible otherwise.

The possibility to grow 2D nano-objects by discharges in liquid nitrogen is an unusual feature of this kind of process. The basic reason of this specific growth mode is yet to be understood. Future studies will concentrate on this key point of interest.

ACKNOWLEDMENTS

This work benefited from the support of the project CEENEMA ANR-15-CE05-0005-01 of the French National Research Agency (ANR).

REFERENCES

[1] M. Cazayous, C. Langlois, T. Oikawa, C. Ricolleau, A. Sacuto, Phys. Rev. B 73 (2006) 113402.

[2] S.J. Kim, E.A. Stach, C.A. Handwerker, Appl. Phys. Lett. 96 (2010) 144101.

[3] M. Tsuji, S. Hikino, Y. Sano, M. Horigome, Chem. Lett. 38 (2009) 518–519.

[4] C.K. Kim, G.J. Lee, M.K. Lee, C.K. Rhee, Powder Technol. 263 (2014) 1–6.

[5] A. Muzikansky, P. Nanikashvili, J. Grinblat, D. Zitoun, J. Phys. Chem. C 117 (2013) 3093–3100.

[6] M. Grouchko, A. Kamyshny, S. Magdassi, J. Mater. Chem. 19 (2009) 3057–3062.

[7] H.T. Hai, H. Takamura, J. Koike, J. Alloys Comp. 564 (2013) 71–77.

[8] S. Chowdhury, V.R. Bhethanabotla, R. Sen, Appl. Phys. Lett. 95 (2009) 131115.

[9] H. Jiang, K.S. Moon, C.P. Wong, In Advanced Packaging Materials: IEEE Processes, Properties and Interfaces, 2005. Proceedings. International Symposium on (pp. 173–177). (2005).

[10] M. Taner, N. Sayar, I.G. Yulug, S. Suzer, J. Mater. Chem. 21 (2011) 13150–13154.

[11] M. Valodkar, S. Modi, A. Pal, S. Thakore, Mater. Res. Bull. 46 (2011) 384–389.

[12] N.R. Kim, K. Shin, I. Jung, M. Shim, H.M. Lee, J. Phys. Chem. C 118 (2014) 26324–26331.

[13] S. Chen, D.L. Carroll, Nano Lett. 2 (2002) 1003–1007.

[14] Y. He, X. Wu, G. Lu, G. Shi, Mater. Chem. Phys. 98 (2006) 178–182.

[15] T. Belmonte, A. Hamdan, F. Kosior, C. Noël, G. Henrion, J. Phys. D: Appl. Phys. 47 (2014) 224016

[16] D. Mariotti, T. Belmonte, J. Benedikt, T. Velusamy, G. Jain, V. Švrček, Plasma Process. Polym. 13 (2016) 70–90

[17] F.H. Hayes, F. H., H.L. Lukas, G. Effenberg G. Petzow, Z. Metallkd. 77 (1986) 749–754.

[18] A. Hamdan, C. Noel, F. Kosior, G. Henrion, T. Belmonte, J. Appl. Phys. 113 (2013) 043301.

[19] A. Hamdan, C. Noël, J. Ghanbaja, J., T. Belmonte. Plasma Chem. Plasma Process. 34 (2014) 1101–1114.

[20] H. Kabbara, J. Ghanbaja, C. Noël, T. Belmonte, Nano-Struct. Nano-Obj. 10 (2017) 22–29.

[21] S. Gražulis, A. Merkys, A. Vaitkus, M. Okulič-Kazarinas,. J. Appl. Crystallo. 48 (2015) 85–91.

[22] D.C. Lin, T.S. Srivatsan, G.X. Wang, R. Kovacevic, J. Mater. Engin. Perf. 16 (2007) 647–654.

CAPTIONS

Figure 1: a) Copper oxide (CuO) nanoparticles synthesized between two Cu electrodes immerged in liquid nitrogen and observed after air exposure at two scales by TEM. b) Silver (Ag) sheets and nanoparticles synthesized between two Ag electrodes immerged in liquid nitrogen and observed after air exposure at two scales by TEM.

Figure 2: TEM image of spherical silver nanoparticles. a) Lower size distribution. b) Higher size distribution.

Figure 3: a) Example of a silver nanosheet made of an assembly of spherical nanoparticles. Within circles: 1D-assembly of nanoparticles forming wires. b) Another example at higher magnification.

Figure 4: a) Low-resolution TEM image of a set of two-dimensional sheets synthesized between $Cu_{28}Ag_{72}$ electrodes immerged in liquid nitrogen and observed after air exposure. The presence of nanorods is sometimes observed. b) Nanoparticles with two size distributions. c) Magnification of an isolated sheet. d) High-resolution image of small-size nanoparticles showing their crystalline structure.

Figure 5: High-resolution TEM images showing a) a spherical copper-rich nanoparticle with its composition profile determined over 4 points, b) a facetted silver-rich nanoparticle with its composition profile determined over 10 points. The average composition of each particle made over all points but the two outermost is ($Cu_{90.9}Ag_{4.1}O_{5.0}$) and ($Ag_{93.8}Cu_{6.2}$).

Figure 6: a) TEM images of two-dimensional nano-object produced from $Cu_{28}Ag_{72}$ electrodes. b) Typical diffraction pattern of two-dimensional nano-object interpreted as the cubic $Ag_{98.5}Cu_{1.5}$ phase (ref. 9016252 of the Crystallography Open Database).

Figure 7: X-mapping of two-dimensional objects shown in the Bright Field image. Ag, O and Cu maps are depicted together with their intensity colour scales whose maximum values are indicated by the given numbers.

Figure 8: Examples of Truss structures produced from silver electrodes (left) and from $Cu_{28}Ag_{72}$ electrodes (right).

Figure 9: a) Large view TEM image showing the presence of nanorods associated with sheets. b) Close view TEM image showing nanorods attached together. c) Overall view of a single wire. d) High-Resolution TEM image of a nanorod showing its crystalline structure.

Figure 10: Selected spectra obtained by optical emission spectroscopy 150 ns and 400 ns after breakdown with silver electrodes or AgCu electrodes.

Figure 11: a) Studied silver-rich single nanosheet. b) Corresponding diffraction pattern showing the presence of two different phases. The circled spots have low intensity and are indexed as the $Ag_{98.5}Cu_{1.5}$ hexagonal phase. The other ones are indexed as the cubic phase of the same alloy.

Table 1: Comparison of the different nano-objects synthesized with either Cu, Ag or CuAg electrodes.

Figure S1: EDX spectrum corresponding to the object displayed in Fig. 2b. The oxygen peak is practically negligible. Quantitative analysis indicates it is 100 at.% pure silver. Copper is due to the TEM grid.

Figure S2: Electron Energy Loss Spectroscopy near-edge fine structures for the Cu $L_{2,3}$. b) Electron Energy Loss Spectroscopy near-edge fine structures for the Ag $M_{4,5}$. Cu, CuO, Cu_2O and Ag spectra are given as reference.

Figure S3: EDX spectrum corresponding to the object displayed in Fig. 7a. Quantitative analysis indicates that it is $Ag_{85.5}Cu_{5.5}O_{9.0}$. The Kα line of nickel is due to the grid.

Figure S4: X-mapping of one-dimensional objects shown in the Bright Field image (same as **Fig.11** right). Ag, O and Cu maps are depicted together with their intensity colour scales whose maximum values are indicated by the given numbers.

Figure S5: 3D plots showing raw time-resolved spectra recorded with either silver electrodes or CuAg electrodes. Time step: 50 ns (from 0 ns at the rear to 550 ns at the front).

Figure S6: Time-evolution of voltage and current signals for Ag and CuAg electrode pairs. Signals are almost identical. The energy deposited varies by less than 1.6% from one situation to the other.

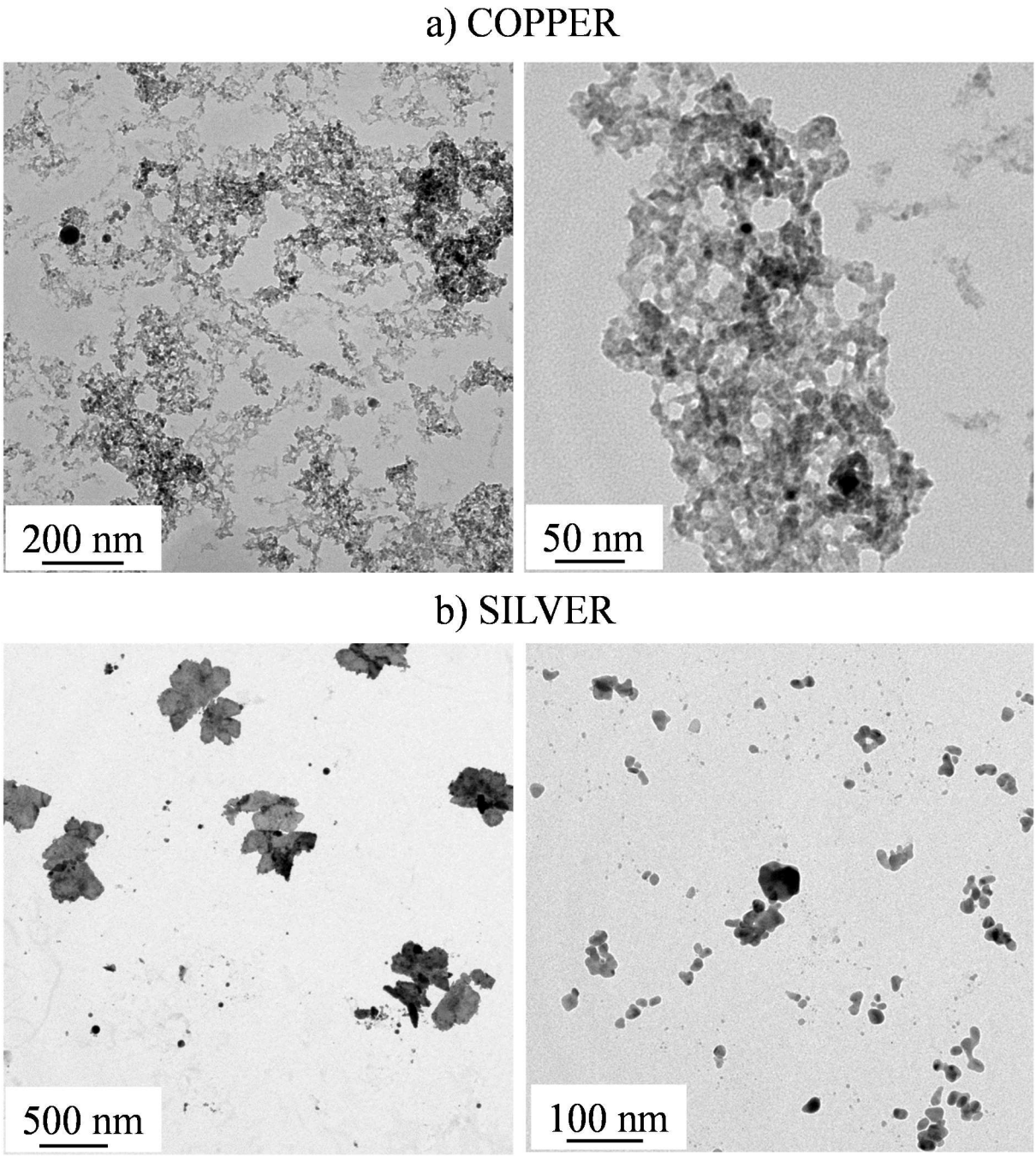

Figure 1: a) Copper oxide (CuO) nanoparticles synthesized between two Cu electrodes immerged in liquid nitrogen and observed after air exposure at two scales by TEM. b) Silver (Ag) sheets and nanoparticles synthesized between two Ag electrodes immerged in liquid nitrogen and observed after air exposure at two scales by TEM.

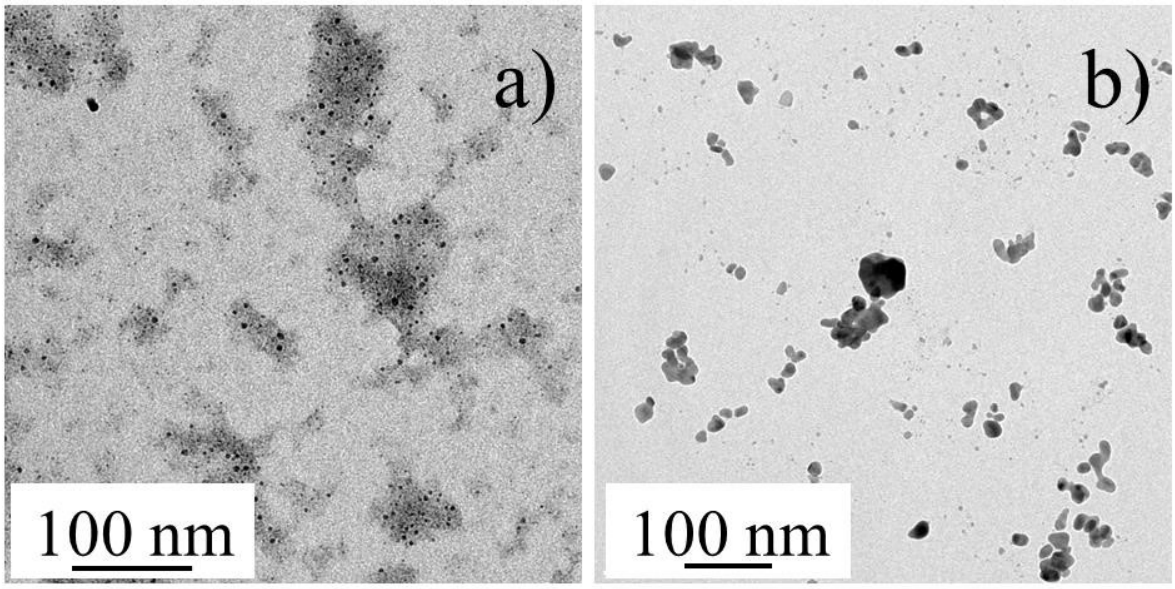

Figure 2: TEM image of spherical silver nanoparticles. a) Lower size distribution. b) Higher size distribution.

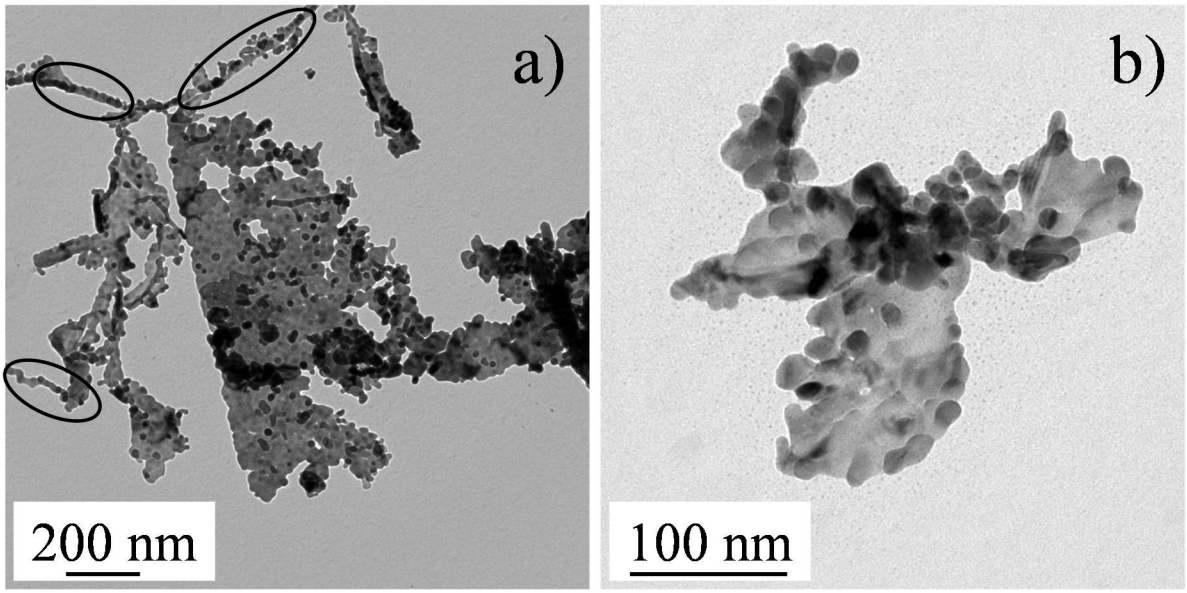

Figure 3: a) Example of a silver nanosheet made of an assembly of spherical nanoparticles. Within circles: 1D-assembly of nanoparticles forming wires. b) Another example at higher magnification.

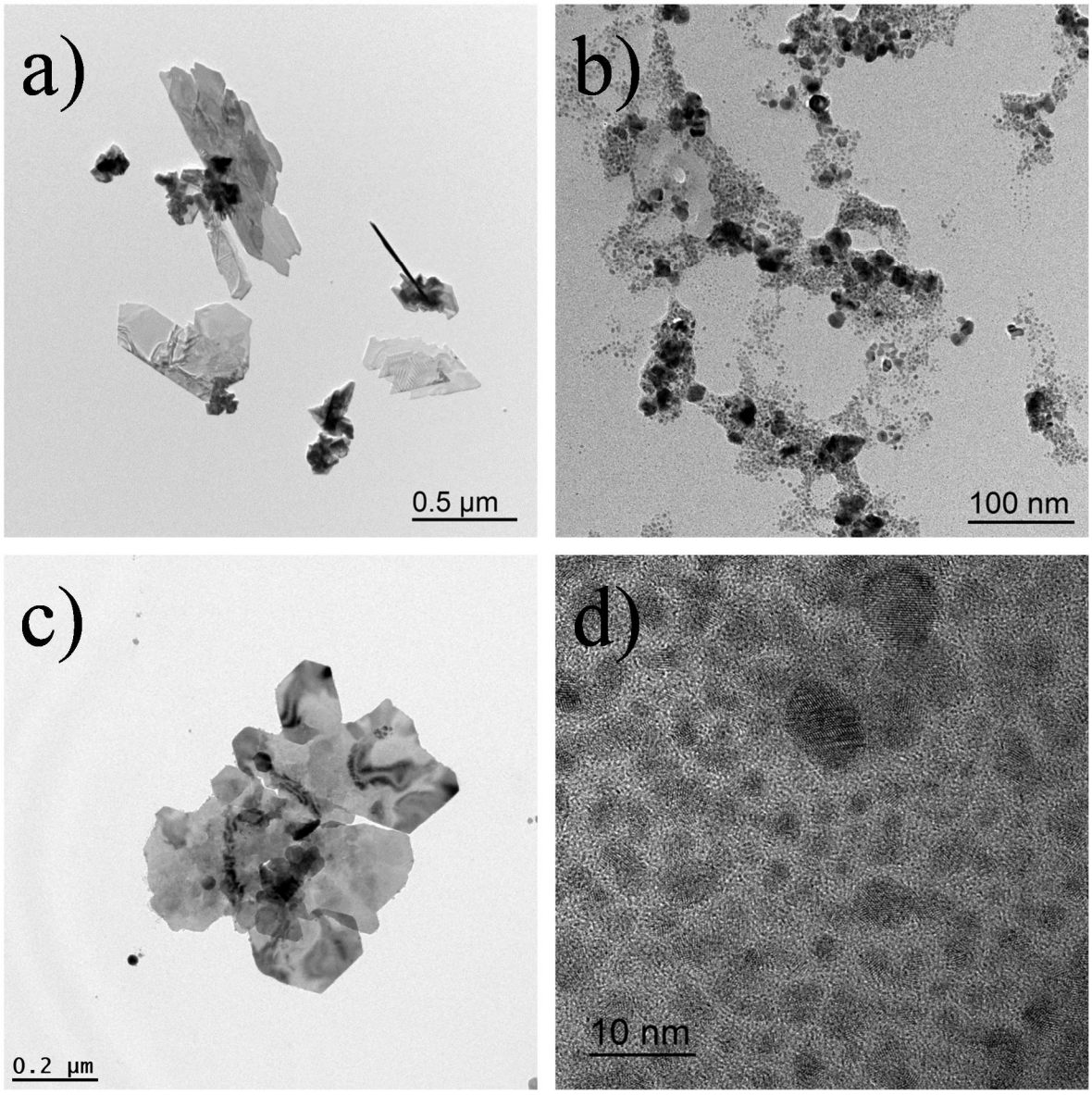

Figure 4: a) Low-resolution TEM image of a set of two-dimensional sheets synthesized between $Cu_{28}Ag_{72}$ electrodes immerged in liquid nitrogen and observed after air exposure. The presence of nanorods is sometimes observed. b) Nanoparticles with two size distributions. c) Magnification of an isolated sheet. d) High-resolution image of small-size nanoparticles showing their crystalline structure.

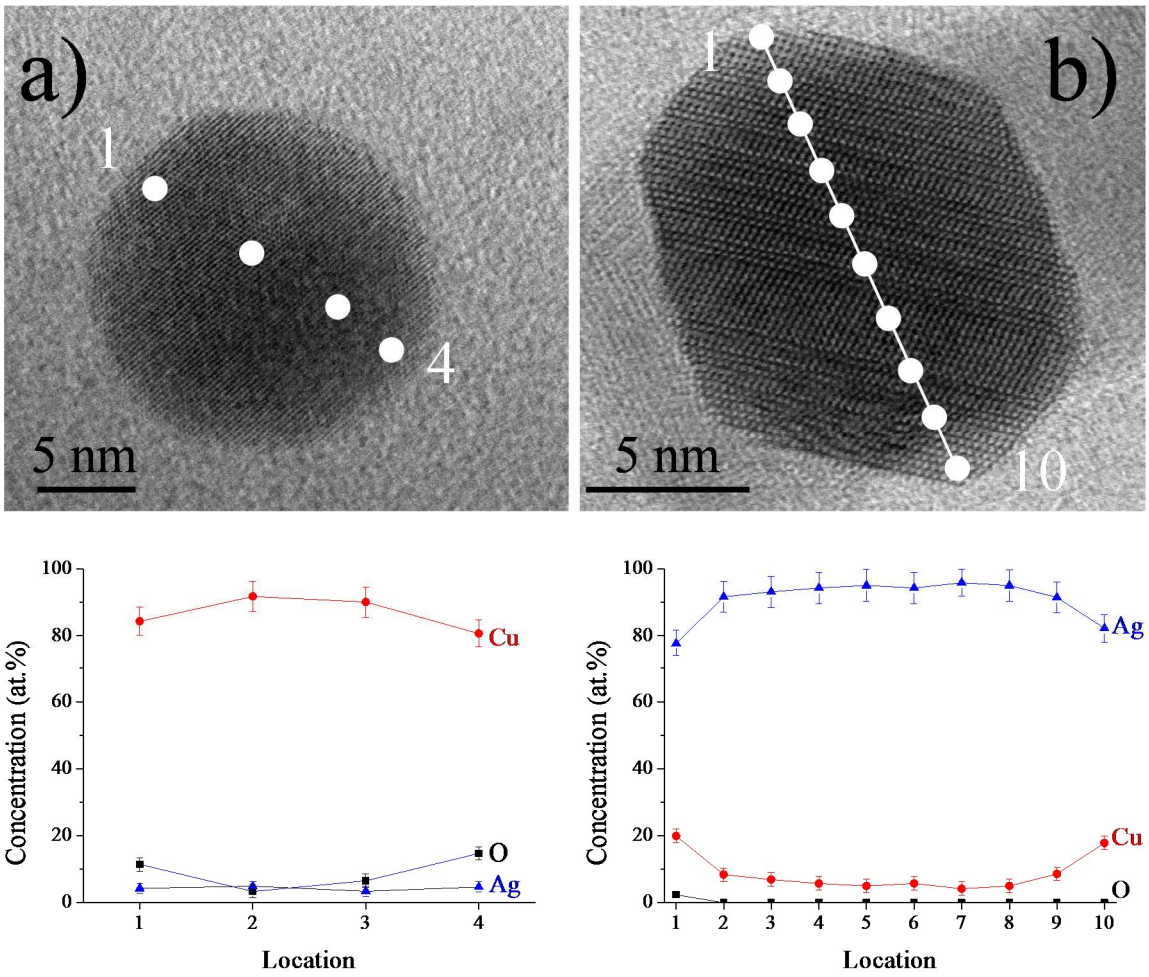

Figure 5: High-resolution TEM images showing a) a spherical copper-rich nanoparticle with its composition profile determined over 4 points, b) a facetted silver-rich nanoparticle with its composition profile determined over 10 points. The average composition of each particle made over all points but the two outermost is ($Cu_{90.9}Ag_{4.1}O_{5.0}$) and ($Ag_{93.8}Cu_{6.2}$).

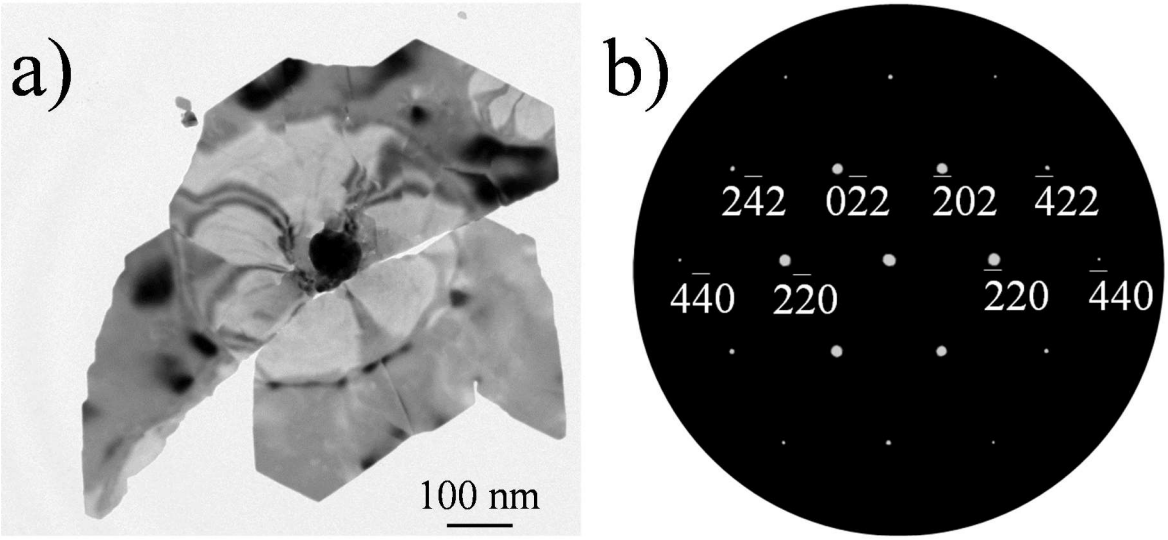

Figure 6: a) TEM images of two-dimensional nano-object produced from $Cu_{28}Ag_{72}$ electrodes. b) Typical diffraction pattern of two-dimensional nano-object interpreted as the cubic $Ag_{98.5}Cu_{1.5}$ phase (ref. 9016252 of the Crystallography Open Database).

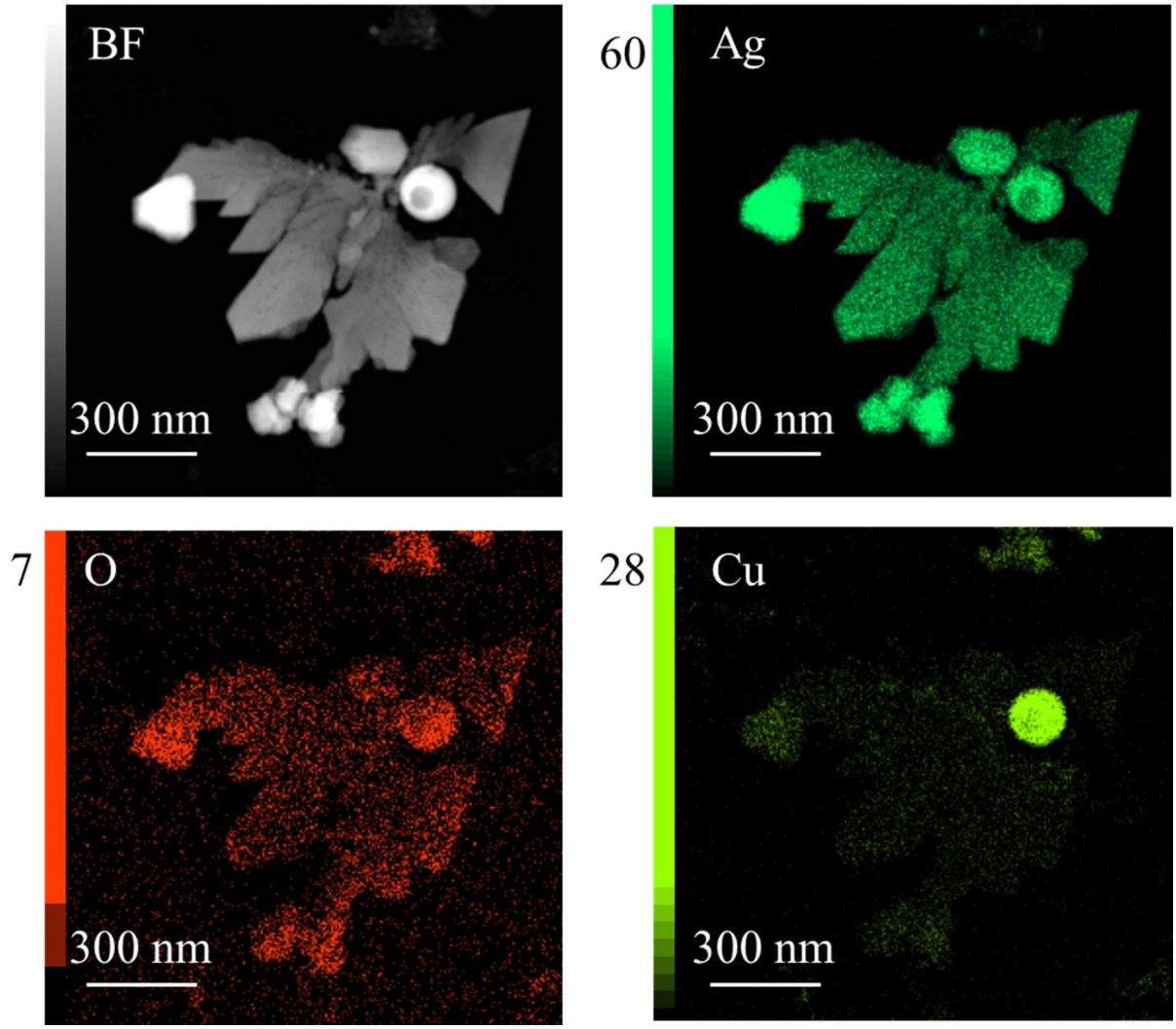

Figure 7: X-mapping of two-dimensional objects shown in the Bright Field image. Ag, O and Cu maps are depicted together with their intensity colour scales whose maximum values are indicated by the given numbers.

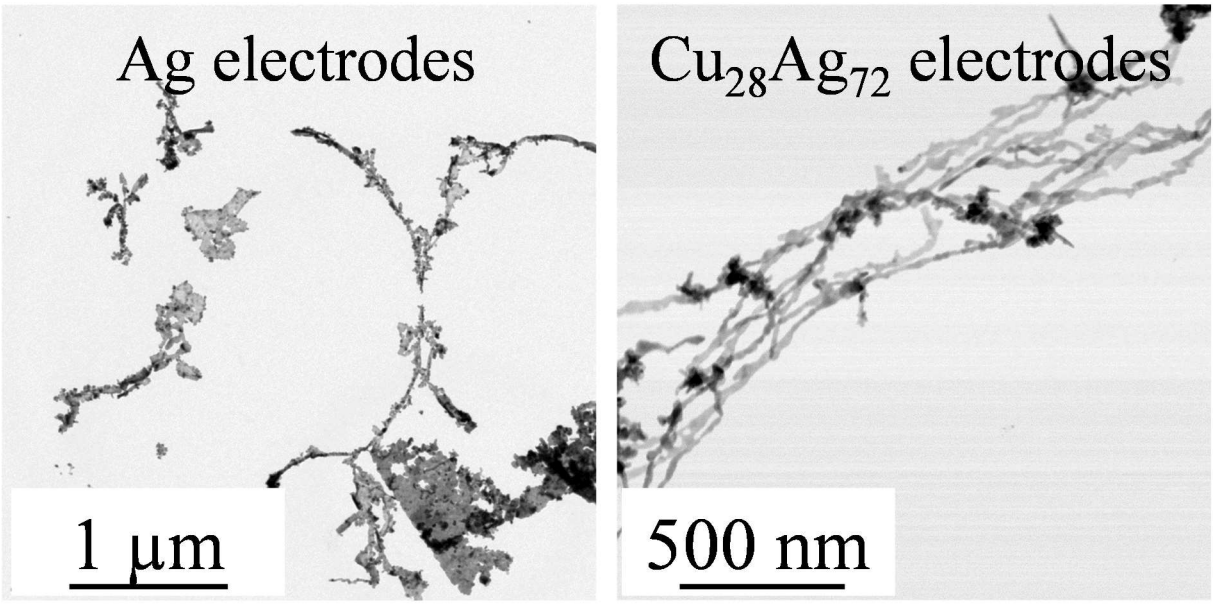

Figure 8: Examples of Truss structures produced from silver electrodes (left) and from $Cu_{28}Ag_{72}$ electrodes (right).

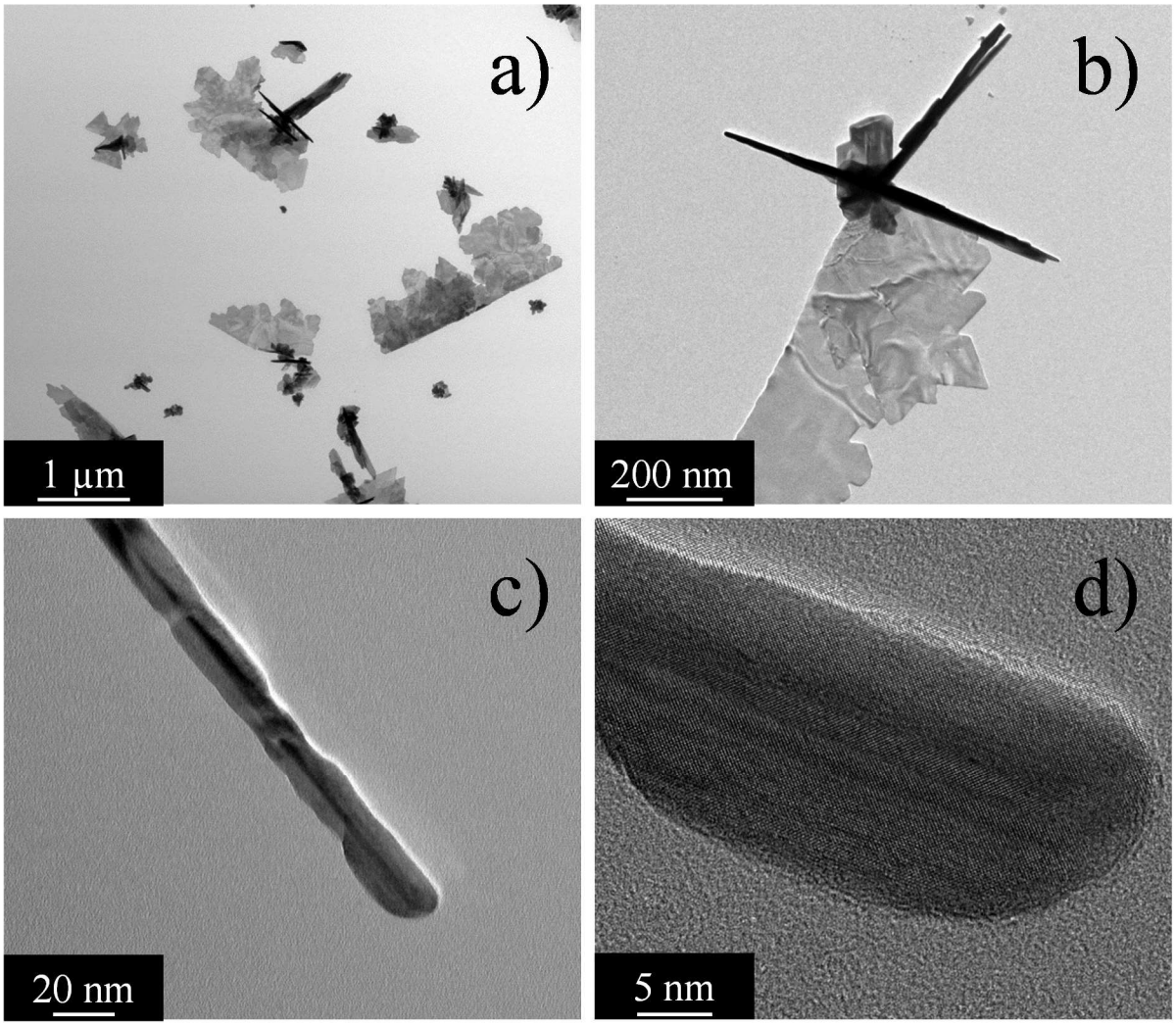

Figure 9: a) Large view TEM image showing the presence of nanorods associated with sheets. b) Close view TEM image showing nanorods attached together. c) Overall view of a single wire. d) High-Resolution TEM image of a nanorod showing its crystalline structure.

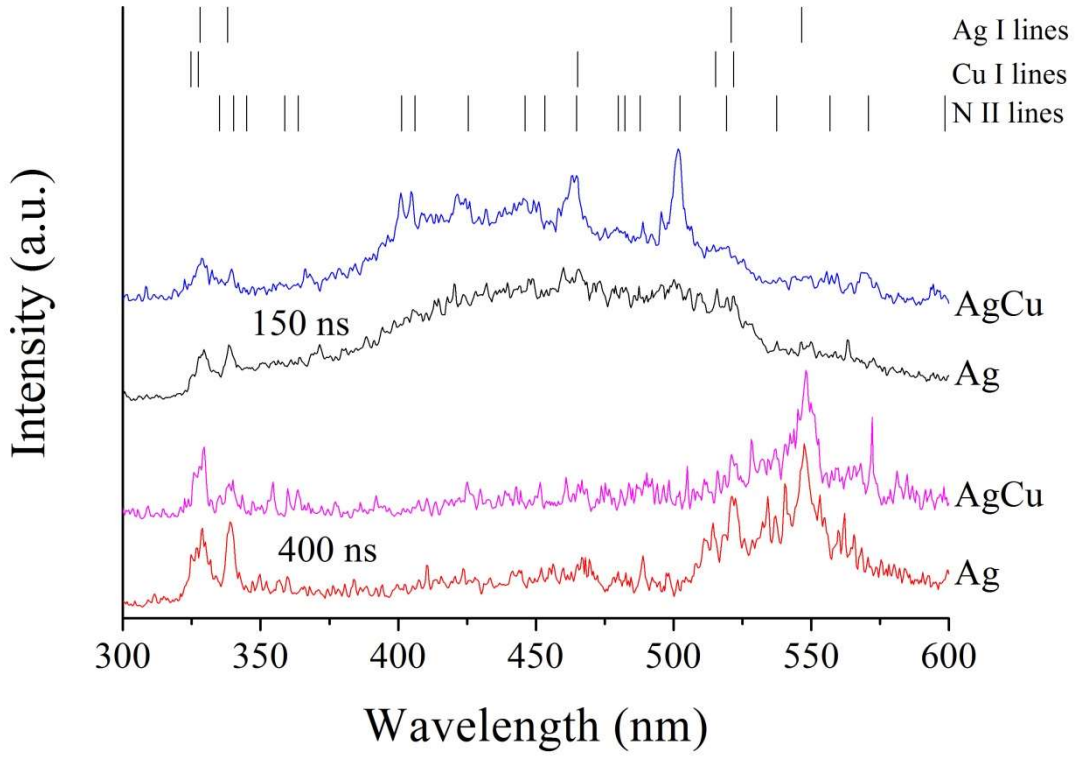

Figure 10: Selected spectra obtained by optical emission spectroscopy 150 ns and 400 ns after breakdown with silver electrodes or AgCu electrodes.

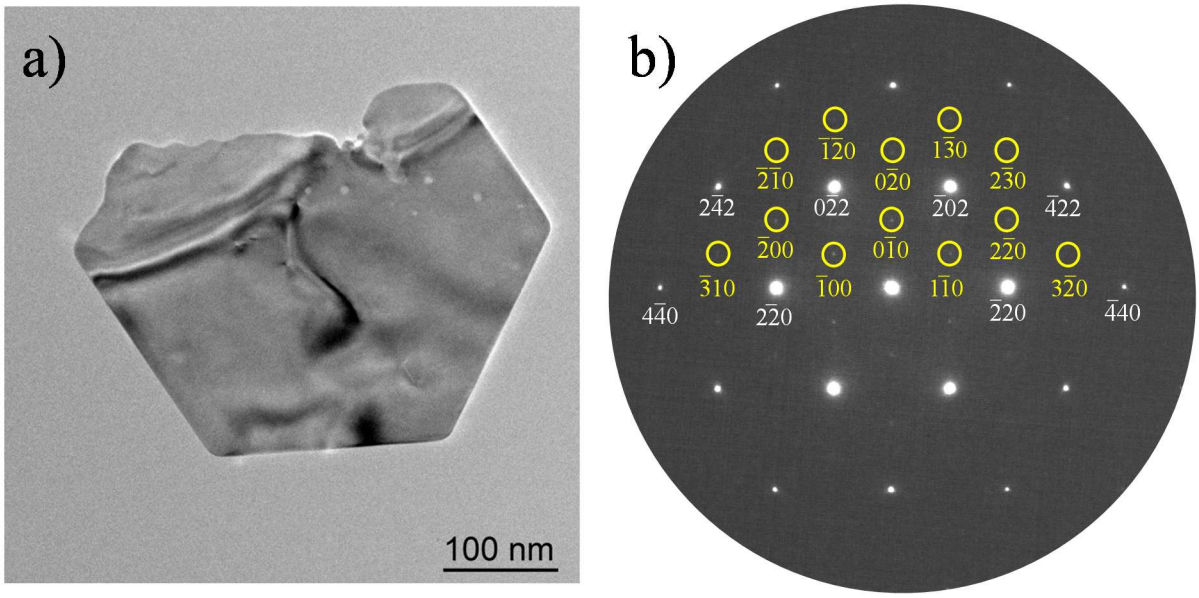

Figure 11: a) Studied silver-rich single nanosheet. b) Corresponding diffraction pattern showing the presence of two different phases. The circled spots have low intensity and are indexed as the $Ag_{98.5}Cu_{1.5}$ hexagonal phase. The other ones are indexed as the cubic phase of the same alloy.

	Cu	Ag	$Cu_{28}Ag_{72}$
Nanoparticles	CuO – Spherical 2–10 nm & 30–50 nm	Ag – Spherical 2–8 nm & 10–30 nm	Cu-εAg – spherical(*) & Ag-εCu – spherical & facetted(*) 2–8 nm & 10–30 nm
Nanorods	–	–	Ag-εCu 100s of nm in length – single crystals
Nanowires	–	Up to several μm in length. Made of NPs of 20 nm	Ag-εCu Up to several μm in length. Made of NPs of 20 nm
Nanosheets	–	100s of nm in width. Made of NPs of 20 nm	Ag-εCu 100s of nm in width – single crystals

(*) ε ~1.5 at.%

Table 1: Comparison of the different nano-objects synthesized with either Cu, Ag or CuAg electrodes.

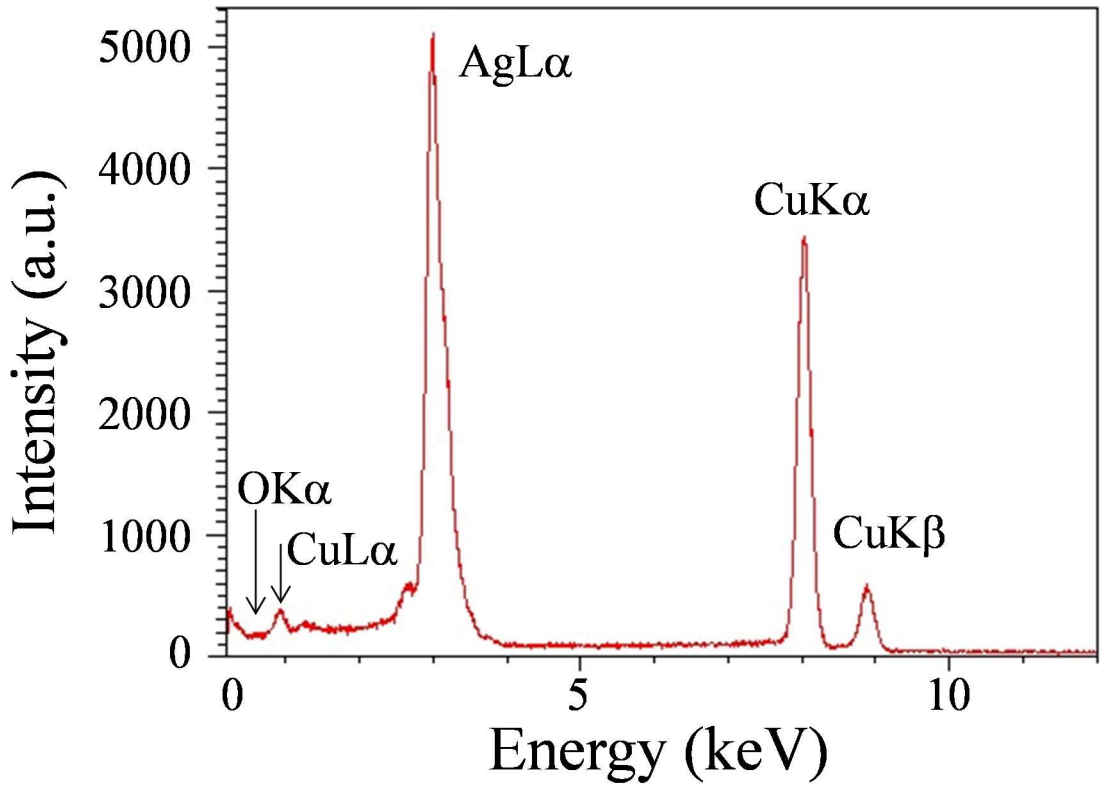

Figure S1: EDX spectrum corresponding to the object displayed in Fig. 2b. The oxygen peak is practically negligible. Quantitative analysis indicates it is 100 at.% pure silver. Copper is due to the TEM grid.

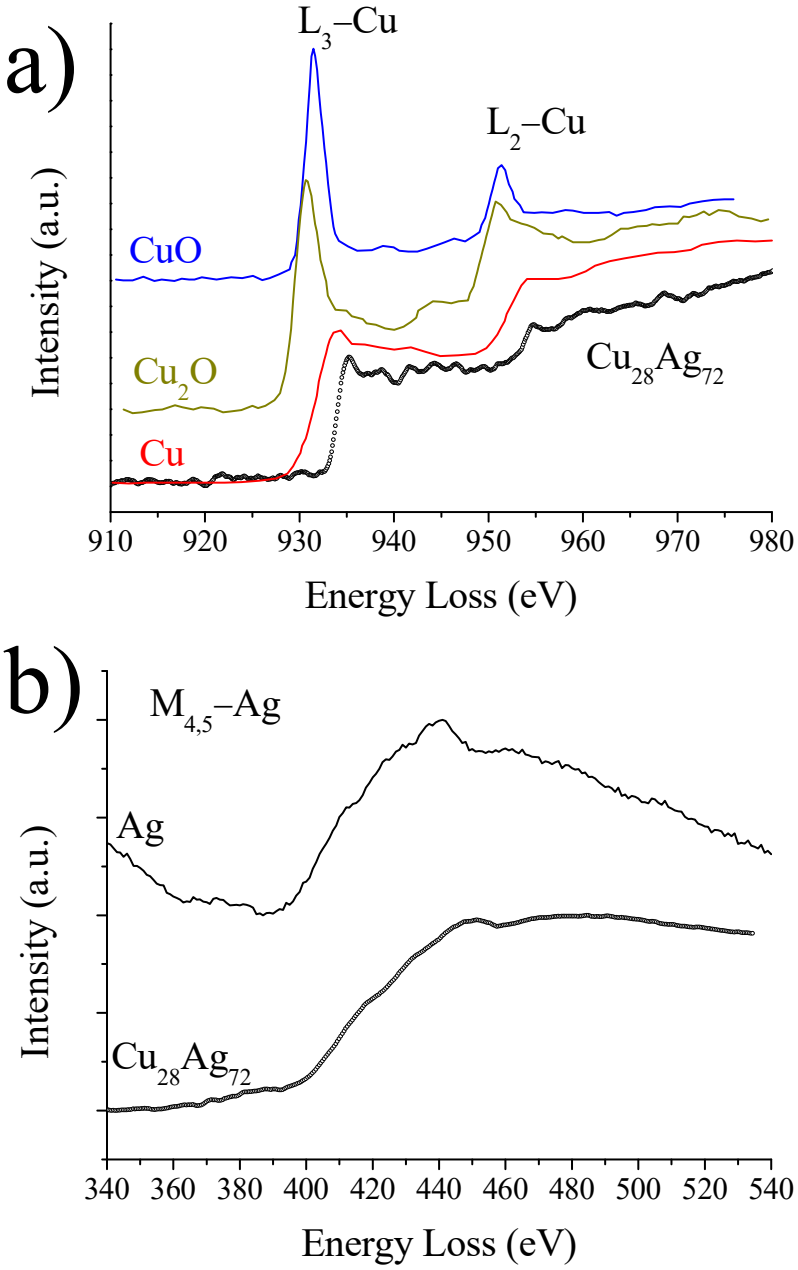

Figure S2: Electron Energy Loss Spectroscopy near-edge fine structures for the Cu $L_{2,3}$. b) Electron Energy Loss Spectroscopy near-edge fine structures for the Ag $M_{4,5}$. Cu, CuO, Cu_2O and Ag spectra are given as reference.

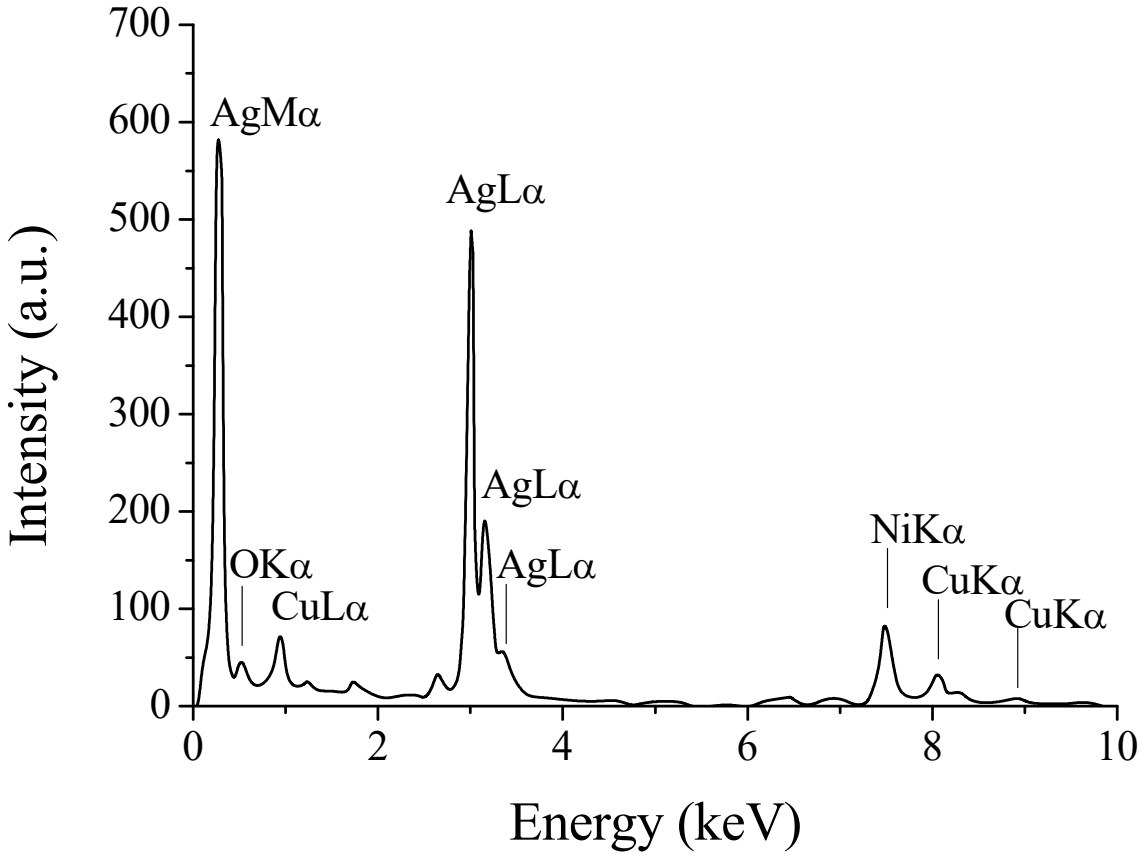

Figure S3: EDX spectrum corresponding to the object displayed in Fig. 7a. Quantitative analysis indicates that it is $Ag_{85.5}Cu_{5.5}O_{9.0}$. The Kα line of nickel is due to the grid.

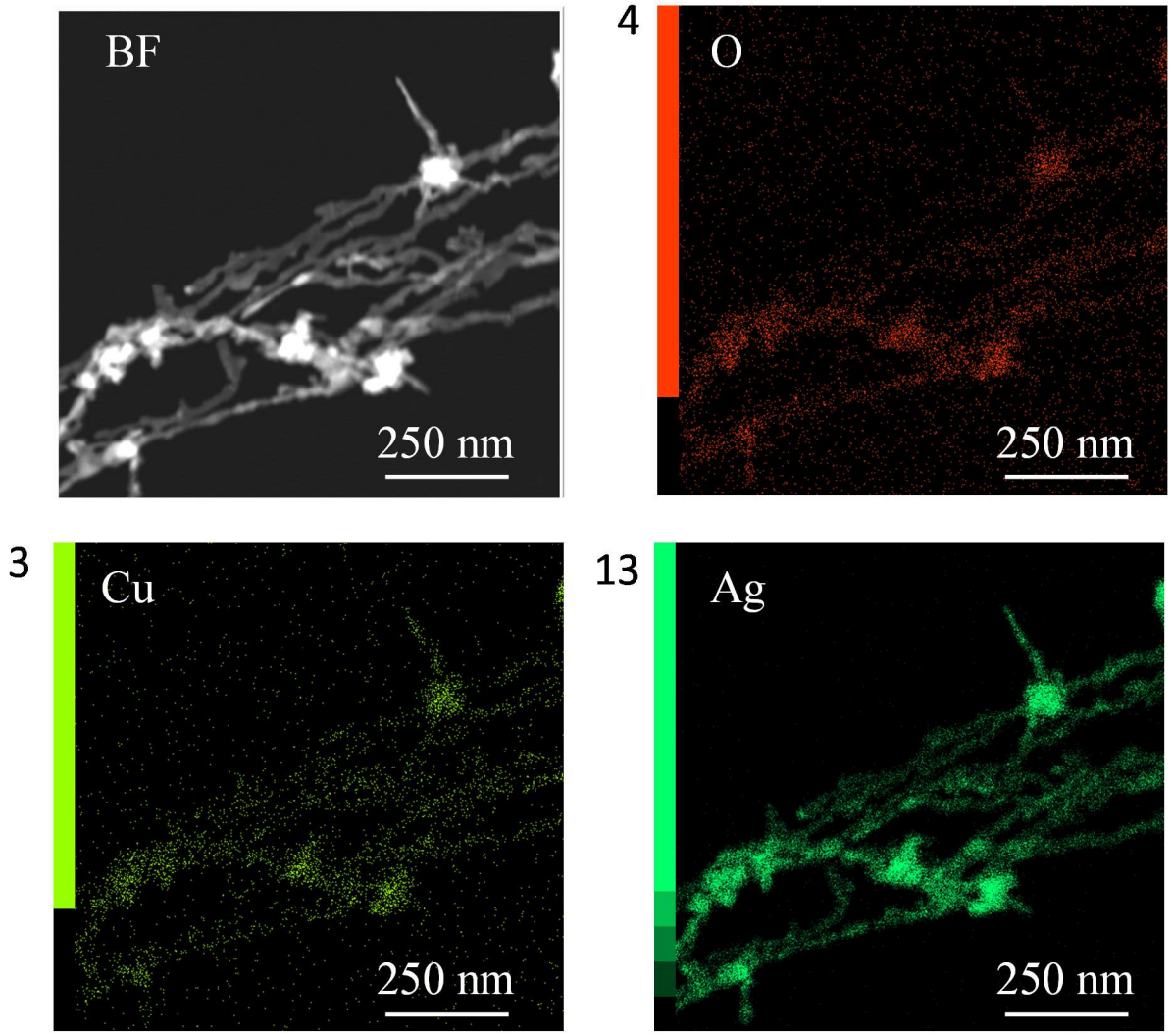

Figure S4: X-mapping of one-dimensional objects shown in the Bright Field image (same as **Fig.11** right). Ag, O and Cu maps are depicted together with their intensity colour scales whose maximum values are indicated by the given numbers.

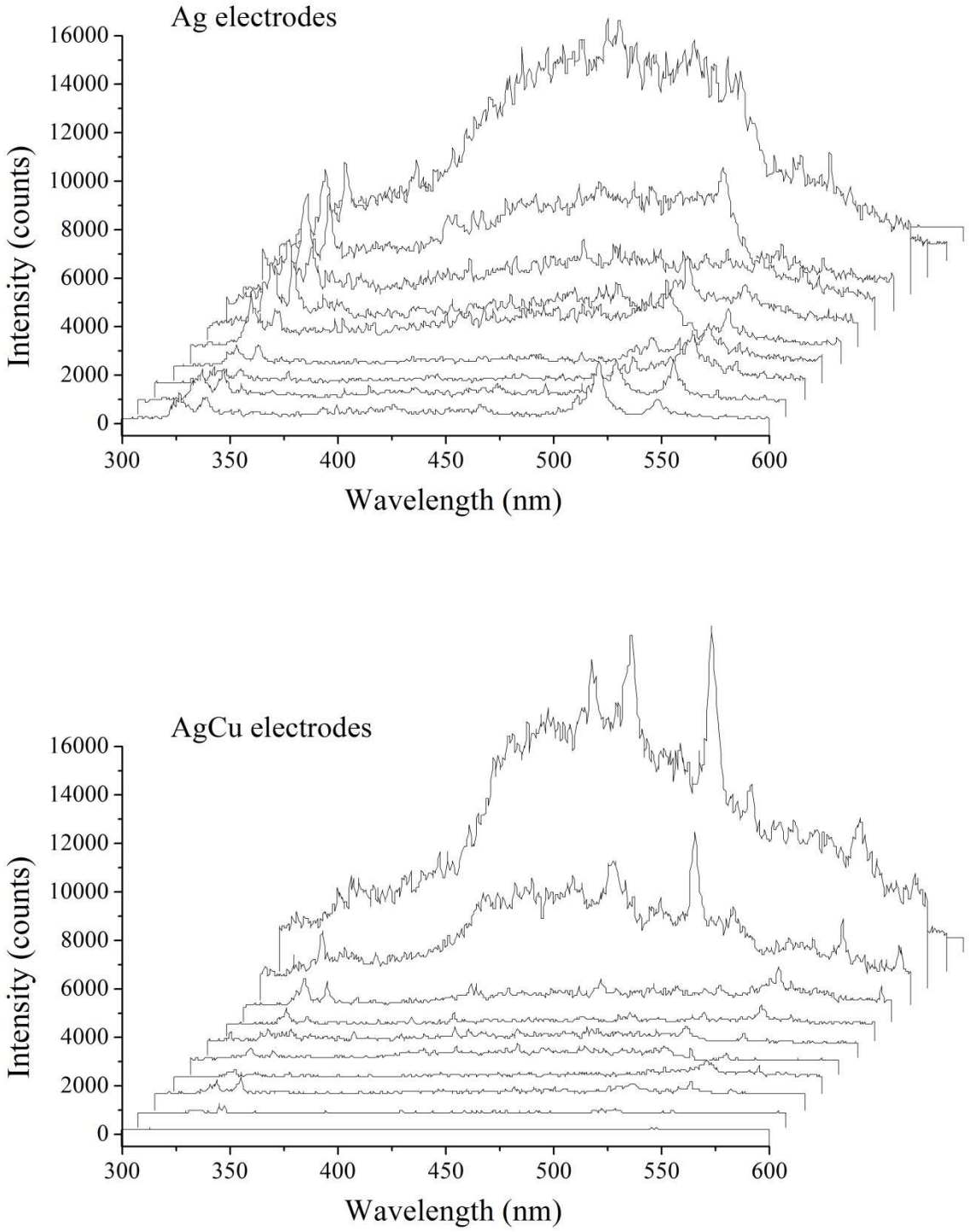

Figure S5: 3D plots showing raw time-resolved spectra recorded with either silver electrodes or CuAg electrodes. Time step: 50 ns (from 0 ns at the rear to 550 ns at the front).

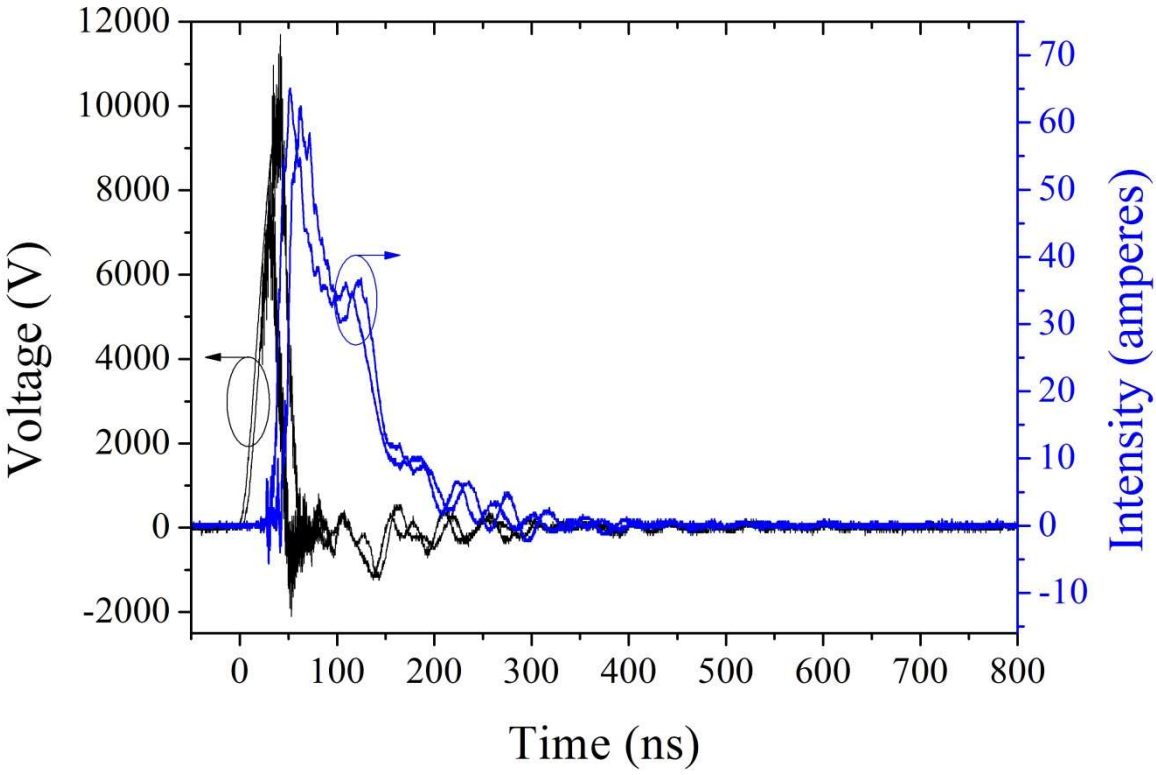

Figure S6: Time-evolution of voltage and current signals for Ag and CuAg electrode pairs. Signals are almost identical. The energy deposited varies by less than 1.6% from one situation to the other.